Transition From a Single to a Double Flame Structure in Swirling Reacting Flows: Mechanism, Dynamics, and Effect of Thermal Boundary Conditions

Proceedings of ASME Turbo Expo 2015: Turbine Technical Conference and Exposition
GT2015
June 15 – 19, 2015, Montréal, Canada

GT2015-43998

TRANSITION FROM A SINGLE TO A DOUBLE FLAME STRUCTURE IN SWIRLING REACTING FLOWS: MECHANISM, DYNAMICS, AND EFFECT OF THERMAL BOUNDARY CONDITIONS

Soufien Taamallah *
Reacting Gas Dynamics Laboratory
Mechanical Engineering Dpt.
MIT
Cambridge, MA, USA

Santosh J. Shanbhogue
Reacting Gas Dynamics Laboratory
Mechanical Engineering Dpt.
MIT
Cambridge, MA, USA

Yinka S. Sanusi
Mechanical Engineering Dpt.
KFUPM
Dhahran, 34464, Saudi Arabia

Esmail M.A. Mokhiemer
Mechanical Engineering Dpt.
KFUPM
Dhahran, 34464, Saudi Arabia

Ahmed F. Ghoniem
Reacting Gas Dynamics Laboratory
Mechanical Engineering Dpt.
MIT
Cambridge, MA, USA

ABSTRACT

We examine experimentally the transition from a single flame stabilized along the inner shear layer (ISL) to a double flame stabilized along both the inner and the outer shear layers (OSL) and spreading over the outside recirculation zone (ORZ) in a fully premixed swirl-stabilized combustor. This work is mainly driven by previous studies demonstrating the link between this transition in the flame macrostructure and the onset of thermo-acoustic instabilities [1, 2]. Here, we examine the transition mechanism under thermo-acoustically stable conditions as well as the dominant flow and flame dynamics associated with it. In addition, we explore the role of changing the thermal boundary conditions around the ORZ and its effect on the presence or absence of the flame there. We start by analyzing the two flames bounding the transition, namely the single conical flame stabilized along the ISL (flame III [1]) and the double conical flames with reactions taking place in the ORZ (flame IV). A dual chemiluminescence approach — using two cameras with a narrow field of view focused on the ORZ — is undertaken to track the progression of the flame as it reaches the ORZ. During the transition, the flame front, initially stabilized along the ISL, is entrained by OSL vortices close to where the turbulent jet impinges on the wall, leading to the ignition of the reactants in the ORZ and the ultimately the stabilization of the flame along the outer shear layer (OSL). This ORZ flame is also subject to extinction when the equivalence ratio (ϕ) is between values corresponding to flames III and IV. For ϕ lower than the critical transitional value, the flame kernel originating from the ISL-stabilized flame is shown to reach the ORZ but fails to grow and quickly disappears. For ϕ higher than the critical value, the flame kernel expands as it is advected by the ORZ flow and ultimately ignites the reactants recirculating in the ORZ. Sudden and extreme peak-to-peak values of the overall heat release rate are found to be concomitant with the ignition and extinction of the ORZ reactants. Finally, Different ther-

*Corresponding author - email: sofiene@mit.edu
[1] Same flame configuration nomenclature as in [1–6]

mal boundary conditions are tested by modifying the heat flux through the combustion chamber boundary, particularly around the ORZ. We find that the transition is affected in different ways: while the transition from flame III to IV (i.e. as ϕ increases) is insensitive to these changes; flame IV persists at lower ϕ as its value is reduced when heat losses through the boundaries are diminished.

NOMENCLATURE

ORZ	Outer or Outside Recirculation Zone.
IRZ	Inner or Inside Recirculation Zone.
OSL	Outer or Outside Shear Layer.
ISL	Inner or Inside Shear Layer.
IR	Infrared
PLIF	Planar Laser Induced Fluorescence.
HS-PIV	High-Speed Particle image velocimetry.
PMT	Photomultiplier Tube.
RMS	Root Mean Square.
ϕ	Equivalence ratio.
α	Thermal diffusivity ($m^2.s^{-1}$).
D_{cb}	Centerbody diameter (m).
g	Velocity gradient (s^{-1}).
S_L^0	Laminar unstretched burning velocity ($m.s^{-1}$).
S_T	Turbulent burning velocity ($m.s^{-1}$).
L_e	Lewis number
K_a	Karlovitz number

1 INTRODUCTION

Modern premixed gas turbine combustors often rely on swirling flow geometries as the preferred way to effectively anchor a flame across a large range of operating conditions. The complexity of such three dimensional flows (presence of multiple stagnation points, low velocity regions, recirculation zones, shear layers as well as potential changes in the hydrodynamic stability) leads to the formation of several flame macrostructures also referred to in the literature as flame shapes or configurations. Several researchers reported the existence of different flame shapes in swirl-stabilized combustion. These have been previously documented as function of fuel composition [7–9], equivalence ratio and preheat temperature [5, 10] and Reynolds number [11], swirl number [12] as well as centerbody geometry [4]. Most of these studies reported the following flames although named differently: a columnar flame (I); a bubble-columnar flame (II); a single conical flame with a flame stabilized along the ISL (flame III); and a double conical flame with an additional continuous flame front stabilized in the ORZ and/or along the OSL (flame IV). The mechanisms underlying these different flames and the transition between them are still not fully understood.

It is commonly conjectured that the change in the burning velocity - the turbulent or the locally strained laminar one - relative to the local flow velocity is the reason why the flame can stabilize in some regions of the flow and not the others. Along the same idea, the extinction strain rate has also been considered as a controlling variable for these transitions [6].
Foley et al. [6] analyzed these transitions for different preheat temperatures and found that when replacing the equivalence ratio (ϕ) and inlet temperature by a calculated extinction strain rate (using the laminar opposed flow extinction model in CHEMKIN) "for the most part, the transitions occur at the same extinction strain rate value" across different operating conditions. A large uncertainty of about 20% to 30% can be seen in the data although considered acceptable by the authors under such experimental conditions.
Guiberti et al. [9, 12] recently performed a comprehensive study focusing on the flame transition between flame III and IV (referred to as V and M flames by the authors). They found that this transition scales with a critical Karlovitz number (K_a). K_a was formulated using an approximation of the velocity gradient close to the wall (g) and a correlation for the turbulent flame speed:

$$K_a = \frac{\alpha\, g}{S_T^2} = \frac{\alpha\, g}{(S_L^0)^2 / L_e^{0.6}}$$

The turbulent flame speed approximations included the Lewis number (ratio of thermal to mass diffusivities) to capture the hydrogen addition effect they studied. Guiberti and coworkers' investigation is one of the few studies that focuses on the transition of a swirling flame to the ORZ. They focused on cases where the flame interacts directly with the wall; they also assumed that the transition occurs through the impingement wall boundary layer by local flashback hence the use of a velocity gradient close to the wall. This velocity gradient reflects the hydrodynamic strain experienced by the flame. By analyzing the effect of fuel, swirl and confinement, they found that the probability of having an M-flame (i.e. flame IV using our nomenclature) increases with the hydrogen volume fraction, and attributed this to the higher propensity of a hydrogen flame to flashback due to larger burning velocity at the same

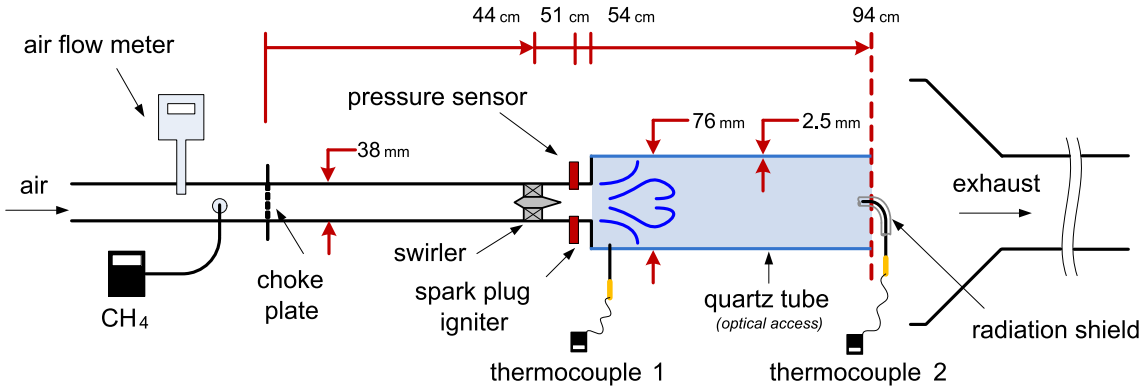

FIGURE 1. Schematic of the swirl-stabilized experimental combustion system.

equivalence ratio and other inlet conditions. However, this modeling approach for the highly wall-dependent transition mechanism investigated by the author was shown to fail when the flame interacts less with the confining wall i.e. in case of larger expansion ratio. This suggests that a different mechanism of flame transition to the ORZ may exist, as also noted by the same authors.

Huang et al. [13] performed large eddy simulations (LES) to investigate flame dynamics in a swirl stabilized combustor. They showed that by increasing the inlet temperature, the flame — originally stabilized along the ISL — flashes back near the wall to reach the ORZ and ultimately stabilizes along the ISL as well, leading to a "tulip" like M-flame. This confirms that flashback through the boundary layer is one of the mechanism delivering combustion to the ORZ and ultimately a flame along the OSL.

In the midst of a more general study looking at the response of different flame shapes to acoustic forcing, Kim et al. [8] also examined the above flame shape transition, although their definition of a V flame is different in the sense that a V-flame extends to the ORZ but without being stabilized along the shear layer. Kim et al. found that the flame angle and length describe very well this transition across different fuels, inlet flow conditions and equivalence ratio, replacing a critical parameter which would be formed using fundamental properties of the flow and fuel by a geometric parameter straightforward to measure in practice.

In addition to the influence of the geometry and several operating conditions on the flame transition to the ORZ, heat loss has been identified as an important mechanism determining whether a flame would be stabilized in the outside recirculation zone and along the OSL. Two studies should be referenced in this regard, one numerical (LES) [14, 15] and one — recently published — based on an experimental investigation of a fully premixed swirl stabilized combustor [9]. Both studies agree on the important role played by thermal boundary conditions and heat losses in the stabilization of premixed swirling flames in the ORZ or along the OSL.

Among the different flame macrostructures observed in swirl-stabilized combustion systems, the transition to an ORZ flame is of particular interest. The main reason remains its close link with the thermo-acoustic stability of the combustor under some conditions [1–3]. Recently, our group highlighted the strong correlation between these flame macrostructures, their transitions and the different thermo-acoustic stability modes observed in a canonical swirl-stabilized combustor. The sharp and sudden bifurcation to a large amplitude limit cycle concomitant with the appearance of the flame in the ORZ under acoustically decoupled conditions suggested that the appearance of the flame in the ORZ may act as a trigger forcing the dynamical system to bifurcate. This justifies and calls for more research effort not only to understand the conditions at which the transition occurs but also the physical mechanisms underlying it.

1.1 PAPER OVERVIEW

The objective of this work is to examine the transition to an ORZ flame and the way it is affected by different thermal boundary conditions. This paper is organized as follows: first, we present the experimental set-up and describe the operating and thermal boundary conditions we explored. This is followed by a description of the different diagnostics tools we relied upon. Then, the instantaneous flame structures acquired using OH-PLIF are analyzed to characterize flame III and IV. These two flame bracket the transition we are examining. Afterwards, the mechanism as well as the rich dynamics of the transition between these two flames are investigated. A novel yet simple approach is employed for this purpose relying on two perpendicular high speed cameras to track the flame front in the toroidal ORZ volume. Finally, we look at the effect of thermal boundary conditions on the critical equivalence ratio at which the flame transitions between flames III and IV.

2 EXPERIMENTAL APPARATUS, OPERATING CONDITIONS, AND DIAGNOSTICS TOOLS

2.1 EXPERIMENTAL SET-UP

The fully premixed swirl-stabilized experimental combustor used in the current investigation is shown in Figure.1. It is similar to the setup used in our recent studies [1, 2]. A circular 38 mm inner diameter stainless steel burner follows a choke plate whose purpose is to prevent acoustic fluctuations from traveling upstream and induce large equivalence ratio fluctuations. It also allows to reach good fuel-oxidizer premixedness. A 2.5 mm thickness fused silica tube with double the diameter of the inlet pipe is used for confinement and optical access. The main addition compared to previous studies include a circular opening centered 10 mm downstream of the expansion plane to allow a K-type thermocouple to be placed through to interrogate the ORZ temperature.

2.2 OPERATING AND THERMAL BOUNDARY CONDITIONS

In the reference case, we operate the combustion system using pure methane with a Reynolds number Re=20,000 and swirl number S = 0.7 with no insulation i.e. a stainless steel side wall and the 2.5 mm thickness quartz tube. The Reynolds number is fixed and defined based on the inlet bulk velocity and diameter. The swirl number is also fixed throughout the paper and is estimated using the expression [16–18]:

$$S = \frac{2}{3}\ \left(\frac{1-(D_{cb}/Din)^3}{1-(D_{cb}/Din)^2}\right)\ tan(\theta)$$

with θ being the fixed blade angle ($\pi/4$), D_{in} the inlet tube diameter (38 mm) and D_{cb} the diameter of the centerbody (9 mm).

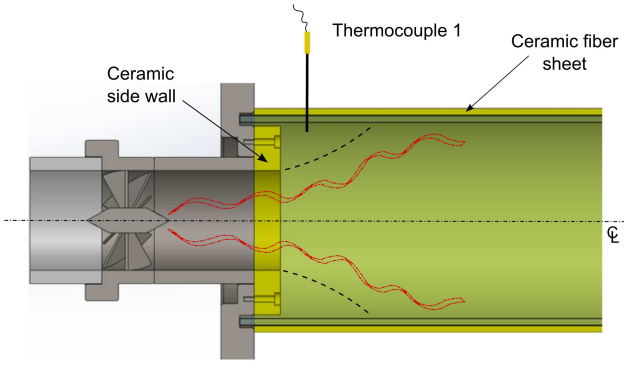

FIGURE 2. Ceramic insulation used to investigate thermal boundary condition effects, and location of the K-type thermocouple probing the ORZ temperature.

The equivalence ratio was varied in the range [0.56 - 0.66] encompassing the transition between flame III and IV at the reference flow conditions. The analysis in sections 3 and 4 is done at this reference case. In the last section of this paper, the investigation of the thermal losses effect includes two additional boundary condition cases at the same Reynolds and swirl numbers (see Figure. 2). A partially insulated case where the stainless steel wall is replaced by a ceramic wall composed of 85% alumina (Al_2O_3) and 15% silica (SiO_2). This material was chosen for its low thermal conductivity of 0.16 $W.K^{-1}.m^{-1}$ at 250°C and 0.29 $W.K^{-1}.m^{-1}$ at 1075°C. The material density and specific heat capacity are 750 $kg.m^{-3}$ and 1047 $J.K^{-1}.kg^{-1}$ respectively, at ambient temperature and pressure. The third boundary condition case is the fully insulated one where, in addition to the ceramic side wall, a flexible ceramic fiber sheet of thickness 5-8 mm is used to cover the quartz tube. The detailed location of the ceramic pieces can be seen in Figure.2. The operating and boundary conditions are summarized in table 1.

2.3 DIAGNOSTICS TOOLS

We relied on multiple optical diagnostics tools: OH Planar Laser Induced Fluorescence (OH-PLIF), chemiluminescence using one or multiple high speed cameras, both intensified and non-intensified, as well as integral CH* chemiluminescence using a photomultiplier.

A Hamamatsu H930602 photomultiplier tube (PMT) was used to record spatially-integrated radiation from the flame at a 10,000 Hz rate. A 50 mm Nikon glass lens was used along with a band-pass filter centered at 430 nm allowing the selective transmission of CH* radical's radiating from the flame. The CH* chemiluminescence fluctuation is normalized by the mean value and considered as a surrogate for the flame heat release [19]. Intermediate and high speed chemiluminescence flame imaging with an infrared (IR) blocking filter (a 2-mm thick CG-BG-39 Schott glass) was performed using two NAC GX-1 high-speed CMOS cameras mounted above and on the side the combustor. The use of two cameras — capturing simultaneously the top and side views — of the combustor was critical for our examination of the ORZ flame transition. Finally, in order to confirm our results and overcome modest signal-to-noise ratio achieved with the cameras mentioned above in low light conditions, we took flame images using an integrated intensified camera from Axiom Optics. The HICAM 5000 Gen 3 camera is equipped with a GaAsP (Gallium arsenide phosphide) photocathode which has a electromagnetic sensitivity window from 350 to 800 nm. This camera was used without an IR filter at a frame of 2000 Hz and an exposure time of 0.25 ms.

PLIF images were acquired by exciting OH species at 283.56 nm wavelength using a Spectra-Physics LAB-170 pump laser with a Sirah Cobrastretch dye laser, circulating ethanol-dissolved Coumarin 153 dye. Fluorescence from excited species

S	Re	ϕ	Thermal Boundary Condition
0.7	20,000	0.56-0.66	Non-insulated : Stainless steel side wall & 2.5 mm quartz tube
			Partially insulated: Ceramic side wall & 2.5 mm quartz tube
			Fully insulated: 2.5 mm quartz tube covered with ceramic sheet

TABLE 1. Operating parameter space and different thermal boundary conditions investigated (the reference case is underlined)

returning to ground energy level was optically filtered and intercepted by a 1280 x 1024 pixel LaVision Nanostar CCD camera. OH-PLIF measurements were performed at a 10 Hz rate with a gating time of 100 ns. A laser beam analysis system including a beam splitter and a Ophir Photonics SP620U CCD camera was used for beam analysis and laser sheet intensity correction of OH-PLIF images.

In addition to optical diagnostics, pressure and temperature measurements were performed. Pressure was measured using Kulite MIC-093 transducers between the swirler and the expansion plane, close to the flame location. A K-type thermocouple was inserted through the quartz tube 10 mm downstream of the sudden expansion side wall and 5 mm into the ORZ (see Figure-2. The thermocouple's sampling frequency is 20 Hz while pressure measurements were performed at 10,000 Hz.

Methane was used as a fuel and supplied by a Sierra C100M Smart-Trak digital mass flow controller with a flow rate uncertainty of $\pm$ 1% of maximum capacity. A Sierra Instruments 780S Flat-Trak flow meter was used to measure the air flow rate with the same uncertainty. Subsequent measurement error on the equivalence ratio was $\delta\phi_{error} \approx 0.002$.

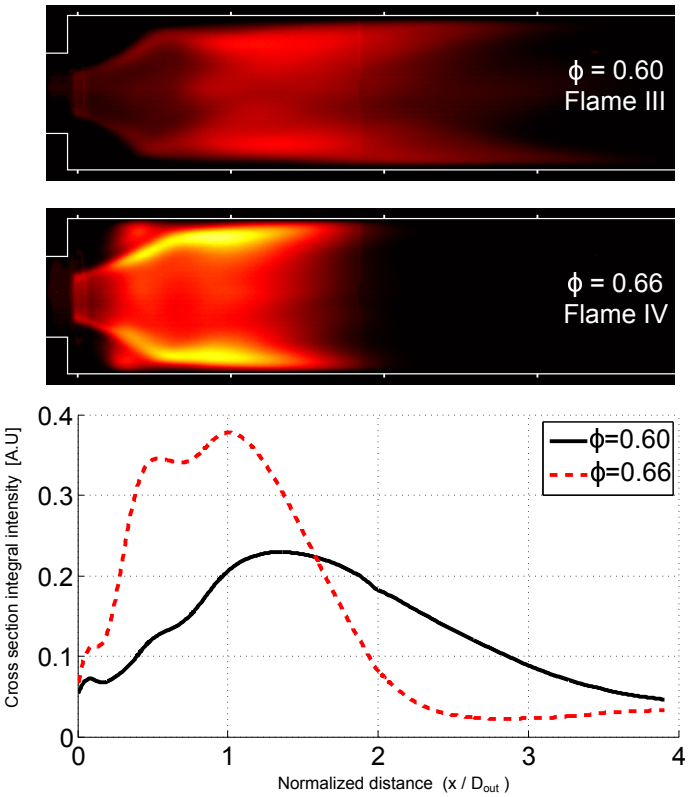

FIGURE 3. Flame III at ϕ=0.6 and flame IV at ϕ=0.66 at the same intensity scale: average of 1800 IR-filtered images taken at 100 Hz and exposure time of 4 ms. Bottom: Integrated intensity along the radial direction.

3 FLAMES III AND IV

In our previous studies using the same combustion test rig, we showed the existence of several flame macro-structures as we changed the equivalence ratio as well as the hydrogen content of the methane fuel mixture [2, 3]. These different flame shapes were also highlighted in several previous studies as mentioned in section-1. These flames included the conical flame (flame III) where the reaction zone is mainly located along the ISL separating the vortex breakdown bubble and the incoming swirling

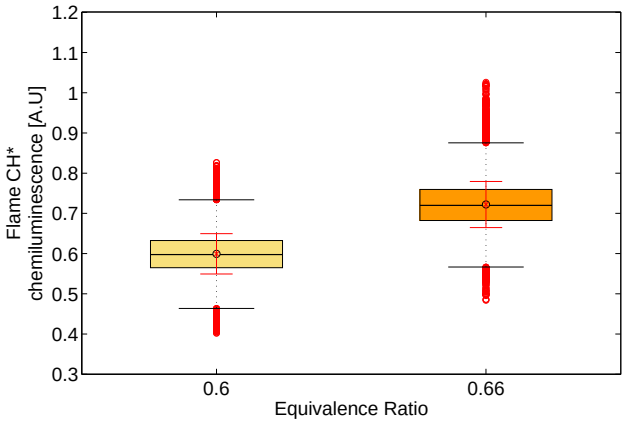

FIGURE 4. CH* radiation statistics from flame III and flame IV: Mean (black circle), median (black line), standard deviation (smaller red whiskers), 25th and 75th percentiles (box edges), approximate 99.3% coverage (larger black whiskers) and outliers (red circles).

jet. Flame IV was shown to appear at higher equivalence ratio or at higher hydrogen content while keeping the same equivalence ratio. The latter flame is characterized by the presence of two flame fronts propagating within the ORZ and eventually but not necessarily along the OSL (also not necessarily extending to the burner lip), besides that propagating along the ISL. These two flames — III and IV — bound the transition we are focusing on in this paper.

Non-Abel transformed chemiluminescence from flame III at ϕ = 0.60 and flame IV at ϕ = 0.66 are shown in Figure-3 for the reference case. These are the results of the averaging of 1800 IR-filtered images taken at 100 Hz and an exposure of 4 ms. After the transition to flame IV, the turbulent flame becomes on average brighter due to the increased heat release at higher equivalence ratio. This can be seen through the location of the maximum radially integrated flame intensity shown in Figure-3-bottom. Figure-3 shows also that the flame becomes more compact. A shorter flame is mainly due to the higher burning velocity and to a lesser extent due to larger flame temperature and its subsequent effect on the flow field. In addition, we see also that when switching from flame III to IV, the location of the maximum moves upstream and a local maximum appears around the jet reattachment location.

The main statistics from the heat release distribution are plotted in Figure-4. These represent flames III and IV CH* radiation as recorded by the PMT and used as a surrogate for the heat

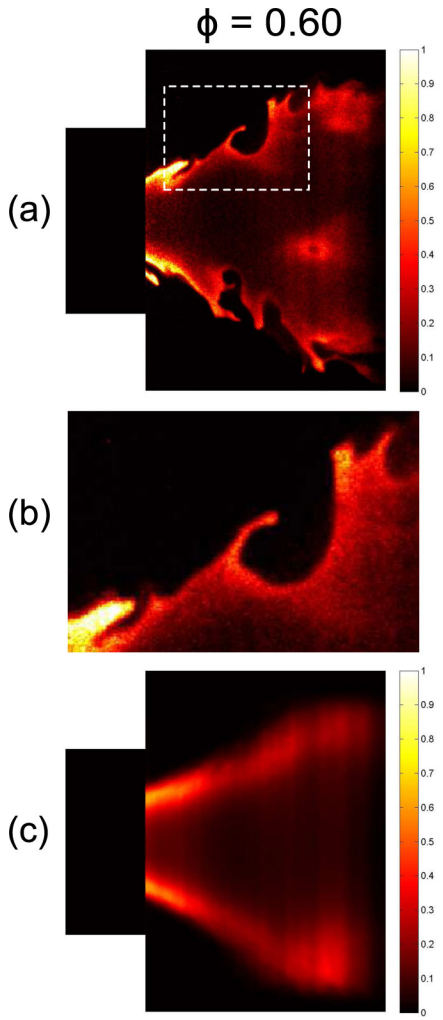

FIGURE 5. OH-PLIF of flame III (ϕ=0.60): (a) a representative OH-PLIF frame with zoom box. (b) zoomed-in box in (a). (c) Mean OH-PLIF of flame III using 256 instanteneous images.

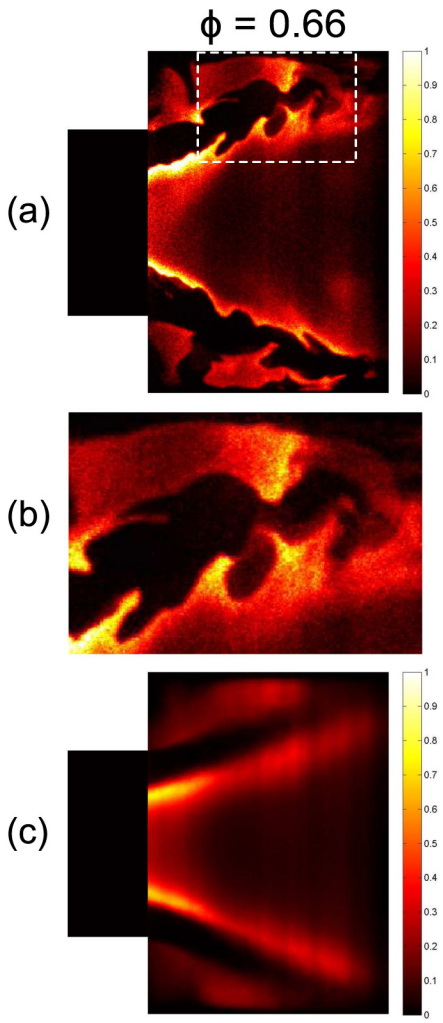

FIGURE 6. OH-PLIF of flame IV (ϕ=0.66): (a) a representative OH-PLIF frame with zoom box. (b) zoomed-in box in (a). (c) Mean OH-PLIF of flame IV using 256 instanteneous images.

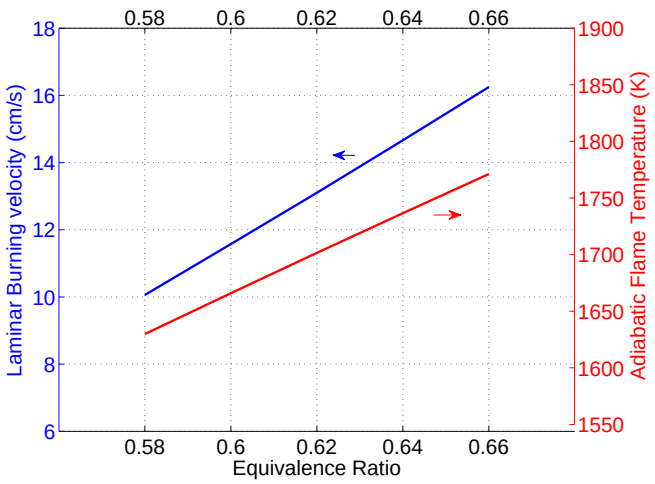

FIGURE 7. Laminar burning velocity and adiabatic flame temperature for the equivalence ratio range of interest, at T=300 K and P=1 atm.

release. The distributions shown include the mean, median, the standard deviation as well as the 25th and 75th percentile levels and finally points considered as outliers. These extreme points represent data falling approximately outside the 99.3% coverage (exactly 99.3% if the data are normally distributed). The average intensity for the two turbulent flames shows the expected increase in the average integral heat release for flame IV due to the higher equivalence ratio. The standard deviation of flame intensity (shown by the smaller red whiskers) is around 8.8% and 7.6% of the mean for flames III and IV respectively while the most extreme values captured by the PMT lie 38% and 42% higher than the mean intensities for flame III and IV, respectively. The above shows that the fluctuations of the heat release around the mean value are of the same order of magnitude despite a significant change in flame macrostructure.

3.1 MICROSTRUCTURES

We examine now the micro-scale structure of the flame or microstructures. OH-PLIF images are taken with a gating time of 100 ns and the spatial resolution of these images is equal to 120 micron per pixel which allows us to extract the detailed instantaneous structure of the flame. OH is present in both the reaction zone and in the products zone as it is slowly consumed in burnt gases compared to it production rate at the flame front [20]. These OH-PLIF raw images were corrected for the spatial non-uniformity of the laser sheet and background noise filtered. Representative OH-PLIF images (a) for $\phi = 0.60$ and 0.66 are shown in Figures 5 and 6 along with a zoom on the reacting flow shear layers (b) and the average OH-PLIF image (c). At $\phi = 0.60$, we see the flame stabilized along the ISL and convoluted by the shear layer vortices. The flame is wrinkled by vortical structures as they form, grow and get convected downstream. The inner diameter of the combustion chamber coincides with the edge of the images shown here. From the flame wrinkling along the sheer layer, it can be inferred that the vortical structures along the ISL have a clockwise rotation in the upper half of the OH-PLIF plane and a counter-clockwise motion in the lower half. This is consistent with the incoming annular jet of reactants with the vortex breakdown bubble's low velocity region inside of it. These vortices are due to the hydrodynamic instability of the ISL vorticity sheet. Moreover, the necessity of a vortex line to close on itself suggests that the upper and lower ISL vortical structures are part of the same helical vortex structure as shown in other studies [13, 21]. This, however, cannot be totally confirmed using only OH-PLIF data due to its two-dimensional nature. In Figure-6.(b), we see that the vortical structures along the ISL have counter-rotating counterparts along the OSL. The latter vortices are also due to roll-up of the combined axial and azimuthal outer shear layer [21]. Figures 5 and 6 show also a wide range of wrinkle sizes; These can be as large as $\approx$ 8 mm in diameter i.e. approximately 1/5 of D_{in} and larger than the methane laminar flame thickness estimated around 1.5 mm at these conditions. Another observation can be made at this point; at $\phi = 0.66$ i.e. when the flame is established in the ORZ with a probability close to one, the flame appears along the OSL and extends deeply inside the recirculation zone region as we can see in Figure-6 (c). In addition, we see the flame intermittently extending to the expansion section along the shear layer.

The two flames described above are the starting and ending point of a transition characterized by the intermittent appearance and disappearance of the flame in the ORZ. We will examine in detail this transition in section 4, but before that it is important to

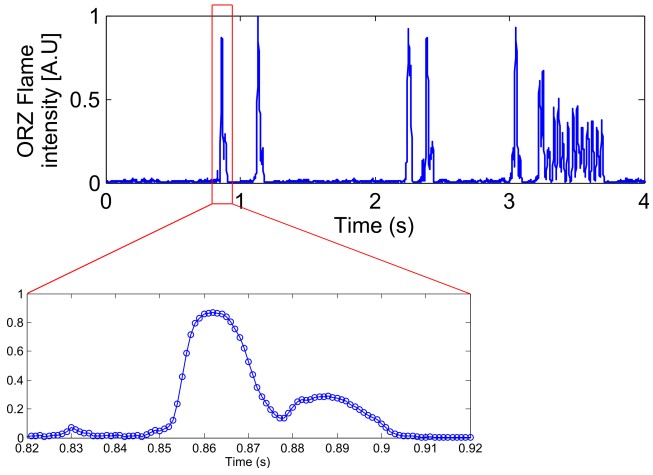

FIGURE 8. ORZ flame intensity as a function of time showing the intermittent appearance and disappearance of the flame in the ORZ (ϕ=0.62).

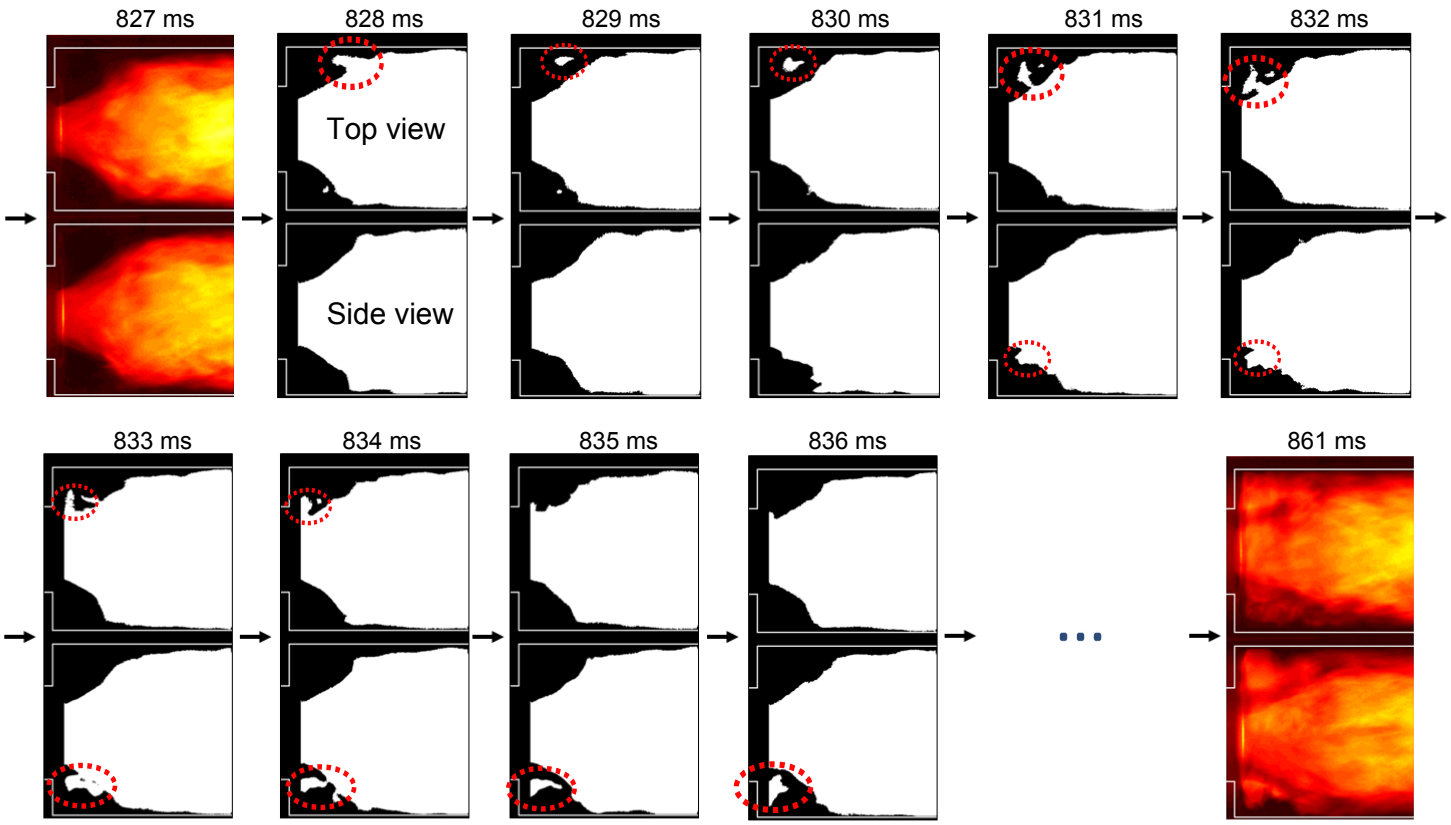

FIGURE 9. Consecutive images taken at 1000 Hz and 1ms exposure time showing the ignition of the ORZ recirculating reactants (ϕ=0.62).

know the fundamental combustion properties, namely the laminar burning velocity and the adiabatic flame temperature (here calculated using CHEMKIN-PRO), for this range of equivalence ratio. These are plotted in Figure-7. The laminar burning velocity increase from of 11.5 cm/s at $\phi = 0.60$ (flame III) to 16.2 cm/s for $\phi = 0.66$ (flame IV). The adiabatic adiabatic flame temperature experiences a less dramatic increases (+11% as compared to 40% for the laminar flame speed) from 1660 K to 1850 K. These two fundamental combustion properties are shown here as a reference at which the transition to an ORZ flame is taking place. Previous high-speed particle image velocimetry (HS-PIV) results performed at the same conditions showed that the root mean square (RMS) velocity at these conditions is of the ranges between 1 and 2 $m.s^{-1}$ i.e. about 10 times the laminar flame speed [1]. Despite their importance, it has been shown that these fundamental quantity do not control the change between these flames III and IV. A burning velocity taking into account hydrodynamic effects like the stretched flame speed ([22]) or the turbulent flame speed ([12]) or the extinction strech rate [6], are more suitable variables potentially governing the transition between flame III and IV.

4 TRANSITION FROM FLAME III to IV

We focus now on the equivalence ratio range between 0.60 and 0.66. This is the range where the intermittent appearance of the flame in the ORZ takes place. In this range, the probability of flame existence in the ORZ increases with the equivalence ratio as previously highlighted [1]. The probability is close to 0 for ϕ=0.60 and equal to 0.99 for ϕ= 0.66 signaling the end of the transition between flames III and IV.

4.1 TRANSITION MECHANISM

The flame intensity in the ORZ region is extracted from a series of high speed images for transitional equivalence ratio range. The intensity is plotted in Figure-8. Large intensity peaks correspond to the appearance of the flame in the ORZ. This is in line with results previously reported [1]. We now look at one of these transitions: the first transition in this data set occurs in the time interval between 0.82 and 0.92 seconds i.e. lasting approximately 100 ms, as shown in more detail in the zoomed-in box in Figure-8. The maximum intensity occurs at t = 861 ms. The corresponding line-of-sight dual flame chemiluminescence i.e. the simultaneous combination of both the top and side

views of the combustor can be seen in Figure-9 ranging from t=827 ms to t=861 ms. Binarized flame images are shown for clarity and to allow easier visual tracking of the flame (brush). At time t=828 ms a flame front extends out of the inner shear layer, at an axial location smaller than the jet reattachment axial location i.e. before reaching the impingement point at the wall. The curved form of the flame front reaching out to the ORZ at t=828 s suggests that it is entrained by a counter-clockwise vortex i.e. an OSL vortex. 1 ms later, a resulting flame kernel appears detached from the ISL flame and start its advection by the ORZ flow. When this flame disappears from the top view, it is captured by the side camera and can be further tracked. At time t=836 ms, the flame kernel becomes larger as it expands while traveling azimuthally along the ORZ torus. This flame motion and expansion continues until the entire ORZ — initially filled with recirculating unburnt reactants — gets ignited and expands the volume of the ORZ while reducing the incoming swirling jet angle as seen at time 861 ms. This time corresponds to the maximum ORZ chemiluminescence intensity highlighted in Figure-8.

This ORZ ignition process — with flame III as an initial condition — repeats 6 times in the 4 seconds of data shown in Figure-8. A major difference can be seen between the first five ignition events and the last one occurring around t=3.2 s. While we observe flame extinction shortly after the entire ignition of the ORZ for the first five ignition events, we see at t = 3.2 s a persistence of the flame; in the latter case, the flame remains in the ORZ for a relatively longer time and keeps rotating inside the ORZ torus around the combustor centerline (from t=3.2 s to 3.7 s) with a clearly defined frequency (as will be described in section-4.2).

Using the two high speed cameras is critical for capturing the mechanism described above, that is the advection of a flame from the ISL by OSL vortical structures causing the sudden ignition of the ORZ. This two-camera approach sheds light on the three dimensional and complex nature of the ORZ and ISL ignition by a flame kernel originating in the ISL. This approach has some limitations and should be complemented with other diagnostics, as only the flame brush with flame motion blur is accessible (due to relatively large exposure time of this method) which means that only a rough image of the flame kernel can be visualized. Moreover, only line of sight data is obtained and the out-of-centerplane motion of an ISL flame front reaching the ORZ (like the one shown in the top view at time 828 ms in Figure-9) cannot be easily inferred.

OH-PLIF is used to complement our examination of the transition to an ORZ flame. Figure-10 shows non-consecutive OH-PLIF images, post-processed similarly to Figures 5 and 6. These images confirm the intermittency of the flame appearance in the ORZ; in Figure-10 (b) the flame does not appear at all in the ORZ, like for flame III. In (a), the PLIF snapshots show a flame

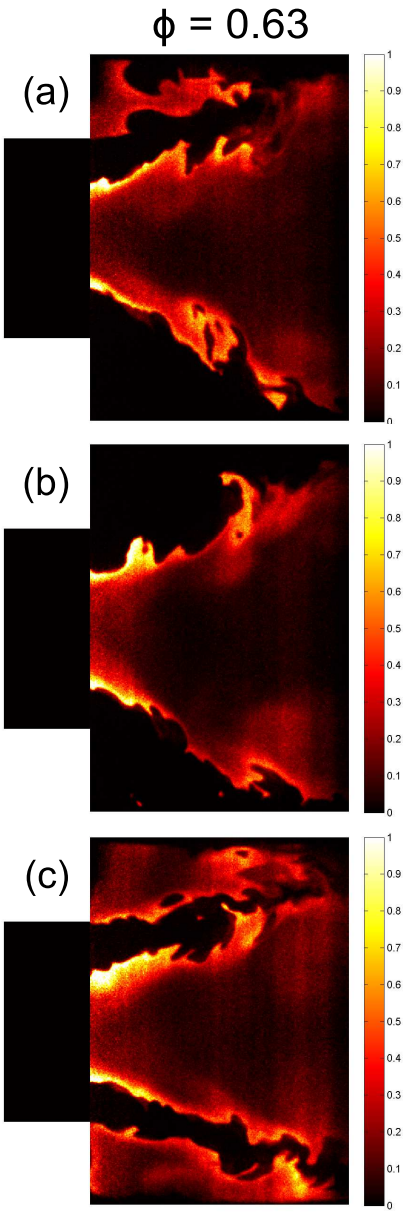

FIGURE 10. Non-consecutive OH-PLIF images of transitional flame III-IV (at ϕ=0.63)

only the upper part of the ORZ with a weakly connected reaction zone between the ISL and the ORZ. Finally, in (c), a flame exists in both sides of the ORZ implying that combustion is taking place throughout this zone. In this case, the flames along the ISL and in the ORZ are connected in the upper part of the PLIF image and disconnected at the bottom part. Figure-10 (b) shows also how the flame is wrinkled by the flow and entrained in a counter-clockwise motion.

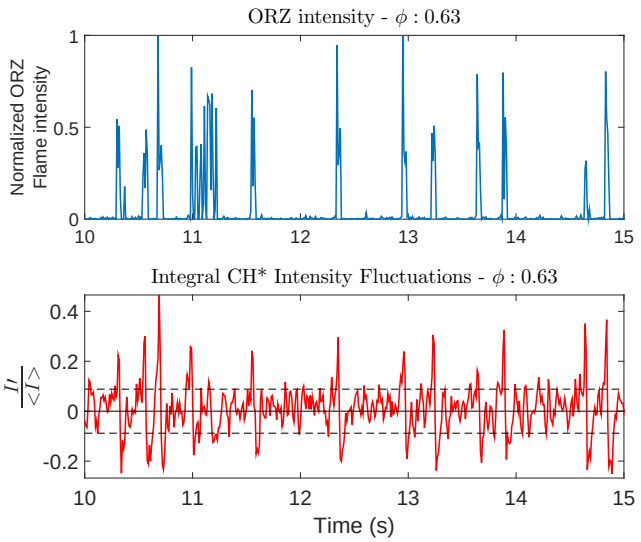

FIGURE 11. Synchronized ORZ-extracted chemiluminescence (top) and normalized integral flame intensity fluctuations (bottom) at ϕ=0.62. Dashed line represents the standard deviation.

The advection of a flame to the ORZ and the subsequent ignition of the recirculating reactants following the mechanism described above is concomitant with the sudden increase in the unsteady heat release. In Figure-11, we can see this correlation as large peak-to-peak fluctuations in normalized chemiluminescence intensity — as the surrogate for normalized heat release — appear simultaneously with spikes in ORZ intensity. This leads to a very different heat release distribution when comparing with both flame III and IV shown earlier (see Figure-4). While the extreme values for flame III and IV were around 40% of the mean intensity, the transitional flame at ϕ=0.63 is characterized by a large number of outliers and by peak values reaching more than 100% of the mean as shown in Figure-12.

This result has potentially important implications for thermo-acoustic stability of combustion systems. Heat release rate fluctuations can non-linearly interact with acoustic pressure fluctuations in a combustion chamber, contributing to an increase in the acoustic energy [23]. The appearance of the flame in the ORZ leading to the ignition of the entire region could act as a triggering mechanism for the onset of instability and the bifurcation to a limit cycle. This can explain the correlations observed between the onset of thermo-acoustic instabilities observed in previous studies [2,10] but further analysis is required to confirm this hypothesis which will be a subject of future investigation.

As we raised the equivalence ratio from that corresponding to flame III, the ignition events in the ORZ started when the ϕ reached a critical value $\phi_{III->IV\ crit} = 0.61$. The ignition of the entire ORZ region starts with a flame kernel entrained from the flame initially stabilized along the ISL. A natural question at this stage is the following: Can the flame reach the ORZ below this critical value ? The answer is shown in Figure-13. The figure displays consecutive images taken at 2000 Hz with an exposure time of 0.25 ms with the intensified high speed camera for an equivalence ratio lower than the critical value: (ϕ = 0.58) < ($\phi_{III->IV\ crit}$ = 0.61), corresponding to flame III. The intensified camera was used to overcome relatively low signal-to-noise ratio at this low equivalence ratio. Even at lower equivalence ratio corresponding to flame III, a flame kernel can occasionally reach the ORZ following the same mechanism as the one described earlier. However, in all these cases the life time of such a kernel does not exceed 2-3 ms. It quickly extinguishes failing to expand, ignite the ORZ reactants and stabilize a flame in that region of the flow.

4.2 DYNAMICS OF THE ORZ FLAME TRANSITION

During the transition of the flame from state III to IV, two major time scales were previously observed [1]. The first is associated with the revolution frequency of the ORZ flow around the combustion chamber centerline. The flame appearing in the ORZ is advected by this flow and this was confirmed by tracking the flame using two high speed camera as shown in the previous section. In our reference condition (Re=20,000, S=0.7) this phenomenon occurs at a frequency f = 28 Hz or a Strouhal number St = $fD_{in}/U_{in} \approx 0.13$, based on the inlet bulk velocity and diameter. The second time scale is related to a lower, relatively broader band frequency in the 5-10 Hz rnage. This low frequency was linked to the cyclical ignition of the ORZ after having mainly unburnt reactants in that zone. In a previous work, through a Dynamic mode decomposition (DMD) analysis [24], we showed

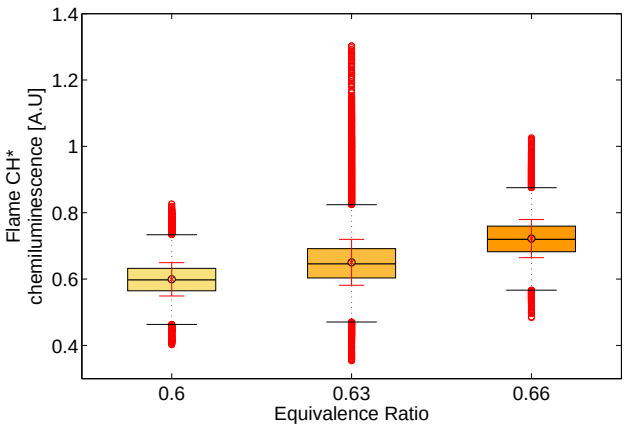

FIGURE 12. CH* radiation statistics for transitional flame (at ϕ=0.63) as compared to flame III and flame IV: Mean (black circle), median (black line), standard deviation (smaller red whiskers), 25th and 75th percentiles (box edges), approximate 99.3% coverage (larger black whiskers) and outliers (red circles).

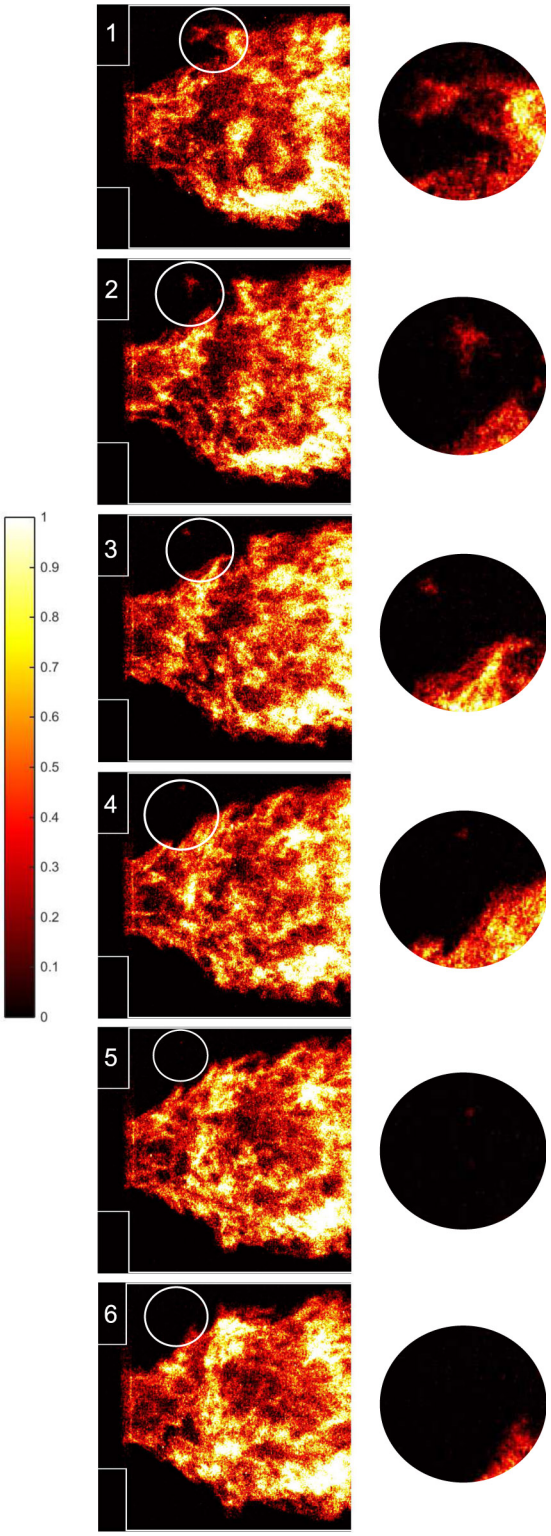

FIGURE 13. Consecutive chemiluminescence images taken at 2000 Hz with an exposure time of 0.25 ms using the HICAM intensified high speed camera at ϕ=0.58 (below the critical $\phi_{III->IV\ crit}$ = 0.61)

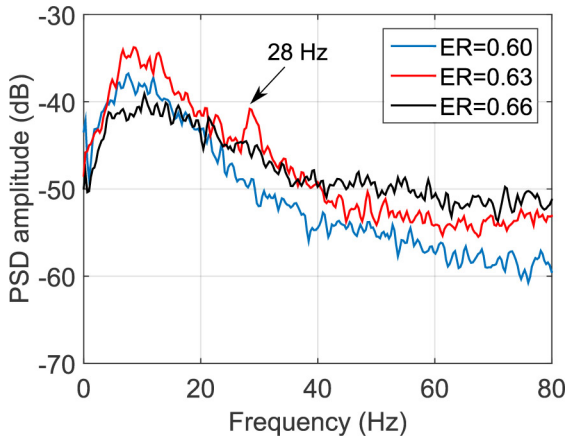

FIGURE 14. Discrete Fourier Transform of the PMT signal from transitional flame (at ϕ=0.63) as compared to flame III and flame IV

that the origin of this frequency band is the flow motion inside the IRZ. In addition, we proposed that this frequency is associated with the cyclical filling and emptying of the vortex breakdown bubble, also previously described by other researchers [25–28] for non reacting flows. By extracting the flame intensity only from the downstream part of the flame and IRZ, the frequency content of the signal shows again the above mentioned low frequency band. This implies that the changes in structures of the IRZ come with an oscillation of the heat release at the same frequencies. Moreover, these oscillations are observed for flame III below transitional values of the equivalence ratio showing that this motion is not specific to the flame during transition III to IV, unlike the ORZ flame dynamics at 28 Hz.

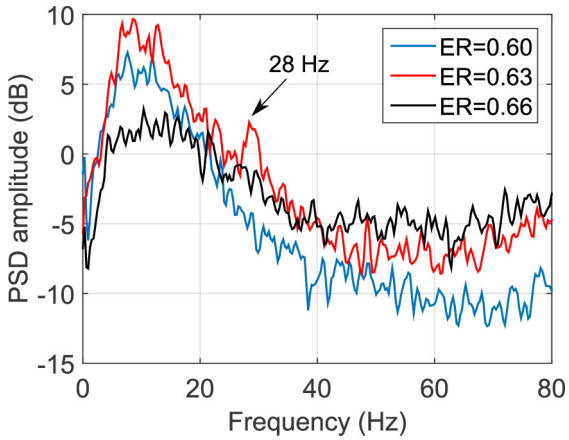

FIGURE 15. Discrete Fourier Transform of the dynamic pressure signal from transitional flame (at ϕ=0.63) as compared to flame III and flame IV

Pressure and integral CH* radiation from the flame were recorded for the transitional flame (ϕ=0.63) as well as flames III and IV at ϕ=0.60 and ϕ=0.66 respectively. Pressure measurements were taken close to the flame, 3 cm upstream of the sudden expansion plane. The Discrete Fourier Transform (DFT) of the resulting signals are plotted in Figures 14 and 15 allowing a direct comparison between flame III, IV and the transitional flame. The flame heat release's frequency content for the three flames shown in Figure-14 is very similar. The signal contains relatively large amplitude components at low frequency around 10 Hz. This frequency is of the same order of magnitude as the low frequency motion of the IRZ described earlier. This confirms that the low frequency dynamics of the IRZ exist for all the flames studied here including flame III and IV and not only the transitional flame. However, a difference can be noticed in the PMT signals DFT shown in Figure-14. A smaller peak at 28 Hz can be seen for the flame at $\phi = 0.63$, which is exactly the same as the revolution frequency of the flame in the ORZ around the combustor's centerline.

The pressure's frequency content for the three flames is analogous to the PMT signal's. A peak at 28 Hz can also be observed for the intermittent flame III-IV and very low frequency band again around 10 Hz is observed. This means that the ORZ flame rotational dynamics has an acoustic signature and sound is radiated from the revolving flame at the same frequency i.e. 28 Hz. The IRZ motion also translates into pressure fluctuations at the same frequency band i.e. around 10 Hz.

5 EFFECT OF THERMAL BOUNDARY CONDITIONS ON THE TRANSITION

When the flame's transition to the ORZ takes place the flame is relatively close to the combustion chamber walls. It is interesting to examine how changes in the heat flux from the reacting flow region to the walls — known to affect flames and their dynamics [9, 14, 15, 29] — would influence this transition and in particular the equivalence ratio at which it occurs. In this section, three cases will be compared. The non-insulated reference

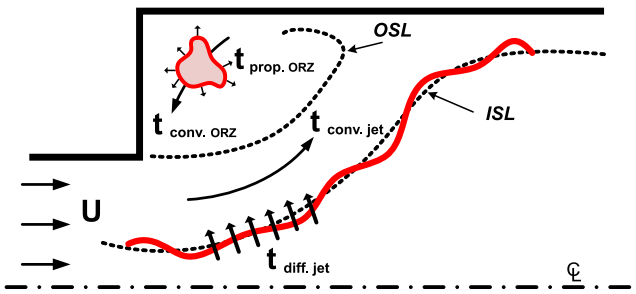

FIGURE 16. Different time scales involved during flame transition III-IV (Diff. :Diffusion, Prop. :Propagation, Conv.: Convection).

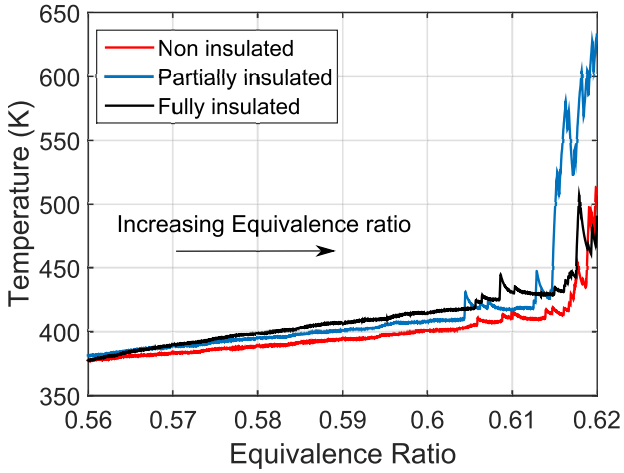

FIGURE 17. Effect of thermal BC on flame transition III to IV as the equivalence ratio is raised.

case as well as the partially and fully insulated combustors, described in section-2.2. The procedure is the following: the equivalence ratio is raised from ϕ=0.56 up to ϕ=0.62 with increment of 0.01 lasting 40 s each to allow a thermal quasi-steady state to be reached. This time lapse is pre-estimated based on the Fourier number of the fully insulated case for which steady state is the longest to be reached. The temperature is continuously measured using the thermocouple inserted 5 mm into the ORZ and placed 10 mm from the side wall, as shown in Figure-2. The same measurements are made while the equivalence ratio is being reduced from 0.62 to 0.56 i.e. from the transitional flame at ϕ=0.62 down to flame III at ϕ=0.56, following the same procedure. In the absence of optical access in this analysis (for the fully insulated case where the quartz tube is covered by the ceramic fiber sheet) the temperature of the outside recirculation zone is used an indicator of the flame presence in that zone. The thermocouple thickness of 2 mm is chosen to minimize the external disturbance of the flow. We also verified that during an ignition and extinction event of the ORZ the flame totally disappears and does not remain anchored to the thermocouple.

Starting from a steady state at ϕ=0.56 (flame III), the unburnt ORZ temperature is recorded around 380 K for flame III at $\phi = 0.56$ (see Figure-17). This temperature rises to 400 K for the non-insulated case and 415 K for the fully insulated case at $\phi = 0.6$ just before the transition. This rise in temperature — before combustion in the ORZ — is due to two parallel mechanisms: the incoming swirling jet is convectively preheated by the flame along the ISL. The degree of preheating in this case results from the competition between two times scales, shown in Figure-16 : the jet convection time and the thermal diffusion time from the flame stabilized in the ISL to the jet. The second mechanisms is the radiation from the products (mainly CO_2 and

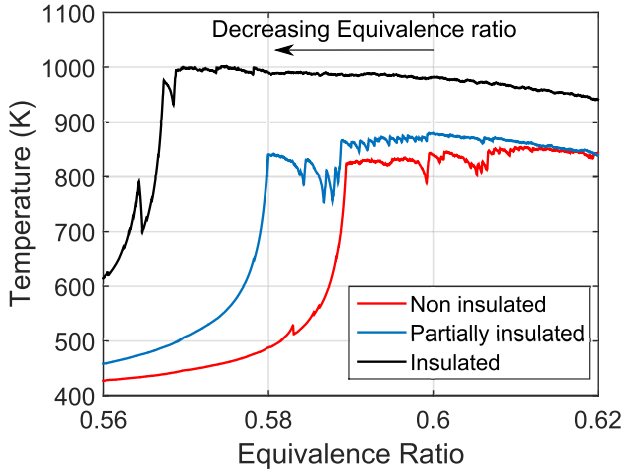

FIGURE 18. Effect of thermal BC on flame transition IV to III as the equivalence ratio is reduced.

H_2O radiation) to heat the ORZ boundaries and these contribute to heating the ORZ reactants.

As we raise the equivalence ratio starting from flame III, spikes in temperature starts to occur signaling the presence of heat release in the ORZ. These spikes i.e. the ORZ flame ignition all start at the same equivalence ratio: ϕ=0.60, independently of the level of heat loss to the boundaries. This indicates that the onset of an ORZ flame is independent of the thermal boundary conditions. A posteriori, this result is consistent with the transition mechanism analysis described earlier: the flame entrainment to the ORZ does not necessarily take place close to the wall. Moreover, while preheating should make the ORZ reactants easier to ignite and stabilize the flame in the ORZ, the change in the preheating temperature across the three boundary condition cases is negligible (400 K for non-insulated and 415 K for fully insulated) compared to the adiabatic flame temperature around the transition (see Figure-7).

Thermal boundary conditions play an important role, however, when a flame is already established in the ORZ and eventually along the OSL. A comparison of Figures 17 and 18 shows indeed that the flame stabilization and extinction are affected differently by the heat flux through the ORZ walls: while the transition from flame III to IV is insensitive to these changes, flame IV, as the equivalence ratio is reduced, persists at lower equivalence ratio when heat flux through the boundaries is reduced. For all cases, a hysteresis effect is observed. For the non-insulated case, the flame completely disappears from the ORZ at ϕ=0.58, whereas it appeared at ϕ=0.6, as seen earlier. This hysteresis is amplified for the fully insulated case; in the latter case, the ORZ temperature is higher. This hotter ORZ flame is at about 1000 K (100 K larger than the non-insulated case)) when first signs of flame extinction start to show; this takes place at ϕ = 0.56.

In summary, Figures 17 and 18 show that the rise/fall of the temperature inside the ORZ, associated with the presence/absence of a flame in this zone occur at different equivalence ratio and depend on whether ϕ is rising or falling. As ϕ increases, on average, the transition to burning in the ORZ occurs at the same value, $\phi \approx$ 0.60-0.61. On the other hand, while ϕ is decreasing, the transition occurs at different values that decrease as the walls are better insulated. Transition occurs at lower ϕ, when decreasing this parameter, due to a hotter and hence more robust flame.

6 CONCLUSION

The goal of this study was to investigate the mechanism underlying the appearance of a flame in the outside recirculation zone in a canonical swirl-stabilized combustor along with its dynamics and the effect of thermal boundary conditions on this transition. We reached the following conclusions:

1. A novel approach using two perpendicular, simultaneous and time resolved chemiluminescence measurements allowed us to elucidate the mechanism through which the flame transitions to the ORZ at higher equivalence ratio. We found that the flame is entrained by vortical structures along the OSL and a reaction kernel reaches the ORZ causing it to ignite. The flame kernel is advected by the ORZ flow as it expands in some occurrences while extinguishing in some other.
2. This flame kernel is an energy source deposited in the ORZ initially filled with reactants. At the critical equivalence ratio corresponding to the onset of the flame transition, it can successfully ignite the entire ORZ reactant region. Below the critical equivalence ratio (flame III), we showed that a flame kernel can still occasionally reach the ORZ, but fails to expand and stabilize a flame in that region of the flow.
3. When successful, sudden ignition of ORZ reactants leads to large fluctuations in the overall heat release rate, which is one of the main characteristic of the transition to an ORZ flame.
4. Reduction in heat losses through the wall boundaries around the ORZ region does not affect the equivalence ratio at which the transition to an ORZ flame occurs starting from flame III. However, the influence of thermal boundary condition becomes significant when transitioning from flame IV to III. With lower heat losses, a hotter and hence more robust flame is observed in the ORZ and this flame persists at lower ϕ as ϕ is reduced.

In future work, we will complement this study by analyzing the instantaneous flow field using HS-PIV and extracting the shear layers vortical structures dynamics. The effect of fuel composition, Reynolds and swirl numbers on ORZ flame transition will also be investigated and modeled.

ACKNOWLEDGMENT

This work was supported by the Center of Clean Water and Clean Energy at MIT and KFUPM (CCWCE) under the grant numbers R12-CE-10, and KAUST University under the grant number KUS-110-010-01.

REFERENCES

[1] Soufien, T., LaBry, Z. A., Shanbhogue, S. J., Habib, M. A. M., and Ghoniem, A. F., 2015. "Correspondence between "stable" flame macrostructure and thermo-acoustic instability in premixed swirl-stabilized turbulent combustion". *Journal of Engineering for Gas Turbines and Power,* ***137***(7).

[2] Taamallah, S., LaBry, Z. A., Shanbhogue, S. J., and Ghoniem, A. F., 2014. "Thermo-acoustic instabilities in lean premixed swirl-stabilized combustion and their link to acoustically coupled and decoupled flame macrostructures". *Proceedings of the Combustion Institute*.

[3] Taamallah, S., LaBry, Z. A., Shanbhogue, S. J., and Ghoniem, A. F., 2014. "Correspondence between uncoupled flame macrostructures and thermoacoustic instability in premixed swirl-stabilized combustion". *Proceedings of ASME Turbo Expo 2014*.

[4] Chterev, I., Foley, C. W., Foti, D., Kostka, S., Caswell, A. W., Jiang, N., Lynch, A., Noble, D. R., Menon, S., Seitzman, J. M., and Lieuwen, T. C., 2014. "Flame and flow topologies in an annular swirling flow". *Combustion Science and Technology,* ***186***(8), pp. 1041–1074.

[5] Chterev, I., Foley, C., Noble, D., Ochs, B., Seitzman, J., and Lieuwen, T., 2012. "Shear layer flame stabilization sensitivities in a swirling flow". *Proceedings of ASME Turbo Expo 2012*.

[6] Foley, C., Chterev, I., Seitzman, J., and Lieuwen, T., 2011. "Flame configurations in a lean premixed dump combustor with an annular swirling flow". In 7th US National Combustion Meeting.

[7] Schefer, R., Wicksall, D., and Agrawal, A., 2002. "Combustion of hydrogen-enriched methane in a lean premixed swirl-stabilized burner". *Proceedings of the Combustion Institute,* ***29***(1), pp. 843 – 851.

[8] Kim, K. T., Lee, J. G., Lee, H. J., Quay, B. D., and Santavicca, D. A., 2010. "Characterization of forced flame response of swirl-stabilized turbulent lean-premixed flames in a gas turbine combustor". *Journal of Engineering for Gas Turbines and Power,* ***132***(4), p. 041502.

[9] Guiberti, T., Durox, D., Scouflaire, P., and Schuller, T., 2014. "Impact of heat loss and hydrogen enrichment on the shape of confined swirling flames". *Proceedings of the Combustion Institute*.

[10] Fritsche, D., Furi, M., and Boulouchos, K., 2007. "An experimental investigation of thermoacoustic instabilities in a premixed swirl-stabilized flame". *Combustion and Flame,* ***151***(12), pp. 29 – 36.

[11] Stopper, U., Meier, W., Sadanandan, R., Stohr, M., Aigner, M., and Bulat, G., 2013. "Experimental study of industrial gas turbine flames including quantification of pressure influence on flow field, fuel/air premixing and flame shape". *Combustion and Flame,* ***160***(10), pp. 2103–2118.

[12] Guiberti, T., Zimmer, L., Durox, D., and Schuller, T., 2013. "Experimental analysis of v to m shape transition of premixed ch4/h2/air swirling flames". *Proceedings of ASME Turbo Expo 2013*.

[13] Huang, Y., Sung, H.-G., Hsieh, S.-Y., and Yang, V., 2003. "Large-eddy simulation of combustion dynamics of lean-premixed swirl-stabilized combustor". *Journal of Propulsion and Power,* ***19***(5), pp. 782–794.

[14] Tay-Wo-Chong, L., and Polifke, W., 2012. "Les-based study of the influence of thermal boundary condition and combustor confinement on premix flame transfer functions". *Proceedings of the ASME Turbo Expo 2012*.

[15] Tay-Wo-Chong, L., and Polifke, W., 2013. "Large eddy simulation-based study of the influence of thermal boundary condition and combustor confinement on premix flame transfer functions". *Journal of Engineering for Gas Turbines and Power,* ***135***(2), p. 021502.

[16] Beeer, J. M., 1983. *Combustion aerodynamics*. Krieger, Malabar, Fla.

[17] Huang, Y., and Yang, V., 2009. "Dynamics and stability of lean-premixed swirl-stabilized combustion". *Progress in Energy and Combustion Science,* ***35***(4), pp. 293–364.

[18] Lefebvre, A., 2010. *Gas turbine combustion : alternative fuels and emissions*. Taylor and Francis, Boca Raton.

[19] Lee, J. G., Gonzalez, E., and Santavicca, D. A., 2005. "On the applicability of chemiluminescence to the estimation of unsteady heat-release during unstable combustion in lean premixed combustor". *AIAA Paper*(2005-3575).

[20] Grisch, F., and Orain, M., 2009. "Role of planar laser-induced fluorescence in combustion research". *Onera Aerospacelab Journal*.

[21] O'Connor, J., and Lieuwen, T., 2012. "Recirculation zone dynamics of a transversely excited swirl flow and flame". *Physics of Fluids (1994-present),* ***24***(7), p. 075107.

[22] Speth, R. L., and Ghoniem, A. F., 2009. "Using a strained flame model to collapse dynamic mode data in a swirl-stabilized syngas combustor". *Proceedings of the Combustion Institute,* ***32***(2), pp. 2993 – 3000.

[23] Nicoud, F., and Poinsot, T., 2005. "Thermoacoustic instabilities: Should the rayleigh criterion be extended to include entropy changes?". *Combustion and Flame,* ***142***(12), pp. 153 – 159.

[24] LaBry, Z. A., Taamallah, S., Kewlani, G., Shanbhogue, S. J., and Ghoniem, A. F., 2014. "Mode transition and

intermittency in an acoustically uncoupled lean premixed swirl-stabilized combustor". In ASME Turbo Expo 2014: Turbine Technical Conference and Exposition, American Society of Mechanical Engineers, pp. V04BT04A061–V04BT04A061.

[25] Lopez, J., and Perry, A., 1992. "Axisymmetric vortex breakdown. part 3 onset of periodic flow and chaotic advection". *Journal of Fluid Mechanics,* ***234***, pp. 449–471.

[26] Brucker, C., and Althaus, W., 1995. "Study of vortex breakdown by particle tracking velocimetry (ptv) part 3: Time-dependent structure and development of breakdown-modes". *Experiments in Fluids,* ***18***(3), pp. 174–186.

[27] Saghbini, J., and Ghoniem, A. F., 1997. "Numerical simulation of the dynamics and mixing in a swirling flow". *AIAA paper*, pp. 97–0507.

[28] Billant, P., Chomaz, J., and Huerre, P., 1998. "Experimental study of vortex breakdown in swirling jets". *Journal of Fluid Mechanics,* ***376***, pp. 183–219.

[29] Hong, S., Shanbhogue, S. J., Kedia, K. S., and Ghoniem, A. F., 2013. "Impact of the flame-holder heat-transfer characteristics on the onset of combustion instability". *Combustion Science and Technology,* ***185***(10), pp. 1541–1567.